Impact of the dopant location in the semi-crystalline structure of alternated donor–acceptor copolymers on the polarity switching p → n mechanism

Bharath Dyaga, Antoine Lemaire, Shubhradip Guchait, Huiyan Zeng, Bruno Schmaltz, Martin Brinkmann

Impact of the dopant location in the semi-crystalline structure of alternated donor-acceptor copolymers on the polarity switching p → n mechanism

Bharath Dyaga,[1] Antoine Lemaire[2], Shubhradip Guchait[2], Huiyan Zeng[2], Bruno Schmaltz[1]

Martin Brinkmann[2]

[1] Laboratoire de Physico-Chimie des Matériaux et des Electrolytes pour l'Energie (PCM2E), EA6299, Université de Tours, 37200 Tours, France.

[2] Institute Charles Sadron, UPR022 CNRS - University of Strasbourg, 23 rue du loess, 67034 Strasbourg, France

Corresponding authors

Bruno Schmaltz : bruno.schmaltz@univ-tours.fr

Martin Brinkmann : martin.brinkmann@ics-cnrs.unistra.fr

Abstract

Strong p-type doping of alternated donor-acceptor copolymers induces p $\rightarrow$ n polarity switching upon progressive band filling, the change of polarity coinciding with the maximum of charge conductivity. This study uncovers the role of the dopant's location in the semi-crystalline structure of the conjugated polymer on the mechanism of polarity switching in highly aligned polymer films of two alternated donor-acceptor copolymers. Using a combination of transmission electron microscopy and polarized UV-vis-NIR spectroscopy, the polarity switching is only observed when the dopants are present in both the crystalline and the amorphous domains of the polymer. This is observed for dopants such as $FeCl_3$. In strong contrast, the dopant magic blue is not able to induce polarity switching because the dopants are not intercalated into the crystals but only in the amorphous phase of the polymer semiconductors. The precise location of dopants in the semi-crystalline structure of a polymer semiconductor is therefore a handle to induce or not the polarity switch and to tune the thermoelectric and charge transport properties of doped polymer semiconductors.

1. Introduction

Large amounts of energy exist in the form of waste heat, solar heat and body heat that might be recovered and transformed to electricity to power electronic devices used for instance in the Internet of Things. Thermoelectric (TE) materials are able to directly convert waste heat in electrical energy. In comparison to inorganic materials, doped polymer semiconductors (PSC) are of high interest for TE applications due to their low cost, ease of processing, tunable electronic properties via macromolecular engineering.[1,2] The thermoelectric performance of the material at a temperature T is determined by the dimensionless parameter $ZT = \sigma S^2 T/k$, σ is the electrical conductivity, *S* is the Seebeck coefficient, κ is the thermal conductivity. Generally, the thermal conductivity in semiconducting polymers is low and in the range 0.1-0.6 W/mK.[3] Optimization of TE properties is obtained by a subtle compromise between optimization of charge conductivity σ, Seebeck coefficient S and thermal conductivity κ of the doped PSCs. As compared to n-type polymer thermoelectric (TE) materials, substantial progress has been made in the last decade in the design of p-type polymer TE materials using various material optimization strategies. To date, electrical conductivities of over 1000 S cm^{-1} and power factors of about 500 μW m^{-1} K^{-2} have been achieved for p-type polymer TE materials.[4-10] One method of choice to prepare effective thermoelectric polymer materials lies in a controlled doping of the originally semi-conducting polymers. There are many different ways to dope PSCs and the doping method and the nature of dopants as well as the polymer backbone and side chains determine the resulting thermoelectric properties of the polymers.[11-14] In strong contrast, the performances of n-type polymer materials lie far behind their p-type counterparts and only a few n-type polymers achieve σ > 10 S cm^{-1} and PF over 100 μW m^{-1} K^{-2}.[15-20] The limited performances of n-type polymers have several origins, to cite but a few: i) inhomogeneous dopant distribution in the

polymer host, ii) the difficulty to dope effectively n-type polymers with a donor-acceptor alternated copolymer structure and iii) poor air stability. The first point i) is encountered when a dopant such as N-DMBI (4-(2,3-Dihydro-1,3-dimethyl-1*H*-benzimidazol-2-yl)-*N*,*N*-dimethylbenzenamine) is mixed with the polymer PNDIT2 (Poly{[*N*,*N*′-bis(2-octyldodecyl)-naphthalene-1,4,5,8-bis(dicarboximide)-2,6-diyl]-*alt*-5,5′-(2,2′-bithiophene)} with limited doping efficiency due to phase separation between PSC and dopant.[21] The second point is a consequence of the limited delocalization of polarons in alternated D-A copolymers.[22,23] Finally, the issue of stability is common to most n-type polymeric TE materials due to the position of the polymer's LUMO and the reactivity of the reduced species with ambient (O_2 and H_2O). Various strategies have been developed to overcome some of the above mentioned issues. For instance, the addition of metallic nanoparticles atop n-type doped PSCs helps improve the stability of the materials via a catalytic reaction of the hydrid generated upon doping of the n-type polymer.[24]

More recently, several groups have demonstrated that a p-type PSC can undergo a p→ n polarity switch of the Seebeck coefficient upon p-type doping with strong oxidants such as $FeCl_3$ or $NOBF_4$.[25-27] In a symmetric manner, n-type polymers were found to undergo switching to p-type upon doping.[28] The origin of the polarity switch has been investigated by various groups in order to identify the key parameters that control it e.g. the chemical nature of the dopant, the doping level, the chemical structure of the p-type polymer (homopolymer *versus* alternated copolymer) and the film morphology (presence of crystalline *versus* amorphous domains). The electronic band filling is one of the parameters ruling the switching mechanism as demonstrated by Zeng et al.[26] A polarity switching from p-type to n-type has been evidenced in oriented films of PDPP5T, a donor–acceptor (D–A) alternated copolymer, upon doping with $FeCl_3$. The switching of the polarity of S was found to coincide with the maximum in charge conductivity σ. After switching, the charge conductivity drops by several

orders of magnitude. Finding the exact doping level leading to the polarity switch is thus essential as it can help fabricating n-type TE materials with optimized TE power factors. As an example, PDPP5T showed a n-type power factors up to 10 μW K^{-2} m^{-1} in oriented films. The previous analysis showed also that the switching of the polarity of the Seebeck coefficient is related to the change of the relative positions of the transport energy and the Fermi energy in the material. Various groups observed similar polarity switching (p-type to n-type or the opposite) in several D-A semiconducting polymers.[25-27] Wang et al.[27] showed that by manipulating the doping level in DPPTTT based D-A copolymer, the Fermi energy shifts from above the HOMO energy to below the HOMO energy of the PSC, explaining the polarity switching from p-type to n-type. Liang et al.[25] investigated the polarity switch in eight different semiconducting polymers doped with $FeCl_3$ and $NOBF_4$. Interestingly, the polarity switching is exclusively observed in highly doped p-type semiconducting polymers with an alternated donor-acceptor copolymer structure and not for homopolymers such as P3HT. The majority of charge carriers was observed to change from holes to electrons at higher doping levels, which was partially supported by Hall effect measurements. Liang et al. proposed that the polarity switching relates to a competition in the charge transport of delocalized electrons in crystalline regions of the polymer at moderate and high doping levels and hopping-type hole transport in amorphous regions.[25] The balance between contributions of charge carriers associated to amorphous and crystalline regions may thus determine the sign of the Seebeck coefficient when both types of charge carriers are present in the samples. Xu et al. proposed that the polarity switching in the n-type polymer BBL is related to the opening of a Coulomb gap when the doping generates multielectronic states i.e. when more than one charge is present per monomer unit.[29]

The objective of this study is to address the possibility of differential doping of amorphous *versus* crystalline domains for two alternated D-A copolymers and its impact on

polarity switching upon doping. We have investigated this possibility for two different D-A copolymers named poly (2Z,5Z)-3,6-bis((2-dodecylhexadecyl)oxy)-2,5-bis(thiophen-2-ylmethylene)-2,5-dihydropyrazine-alt-(E)-1,2-di(thiophen-2-yl)ethene **(PAQM2T-TVT)** and poly (E)-2,5-bis(2-dodecylhexadecyl)-3,6-di(thiophen-2-yl)diketopyrrolo[3,4-c]pyrrole-1,4-dione-alt-(E)-1,2-di(thiophen-2-yl)ethene (PDPP2T-TVT) (**PDPP2T-TVT)** (the chemical structures are shown in Figure 1). Both polymers have the same donor unit i.e., (E)-2-(2-(thiophen-2-yl) vinyl)thiophene (TVT) that was copolymerized with two different acceptor units with different electron-withdrawing abilities. Details of the synthesis and characterization of **PAQM2T-TVT** polymer is found in the literature[30] and the monomers **8**, **9** and **PDPP2T-TVT** polymer are synthesized according to the literature[25,31] and details can be found in SI (Figures S1-S3). Cyclic voltammetry analysis reveals that both polymers have nearly identical HOMO energy levels (figure S2) at -5.48 and -5.50 eV respectively for **PAQM2T-TVT** and **PDPP2T-TVT**.

As dopants, we used two different dopants $FeCl_3$ and magic blue (MB). $FeCl_3$ was chosen as it can dope both crystalline and amorphous domains of PSCs such as PBTTT, P3HT or PDPP5T. [10,26] As a second dopant, we used Tris(4-bromophenyl)ammoniumyl hexachloroantimonate also called Magic Blue (MB) that is sufficiently strong to allow for the doping of D-A semiconducting polymer.[32,33] Zhong et al. studied the doping mechanism of oriented P3HT films with MB.[34] They recently demonstrated that MB does not enter the crystals of P3HT. Doping occurs via the interface with the amorphous phase and thus MB dopants are located preferentially inside the amorphous zones of P3HT. The authors demonstrated that by doping P3HT from the amorphous zones, the crystal structure is preserved and hence, high conductivity over 3000 S cm^{-1} is obtained. The fact that MB is essentially located in the amorphous phase of a PSC is thus taken as an opportunity to probe the impact of dopant location in amorphous *versus* crystalline PSC phases on the occurrence

of the polarity switching in low bandgap polymers. Finally, to realize this study, we used oriented PSC films that ease the study of doping of amorphous versus crystalline zones using for instance polarized UV-vis-NIR spectroscopy. When the incident light polarization (POL) is parallel to the rubbing direction (chain direction), absorption is mainly from ordered and aligned crystalline PSC domains whereas for POL⊥R, light is mainly absorbed by amorphous zones. The absence of polaronic signatures for doped polymer films POL⊥R is thus an indication that amorphous zones are little or not doped, e.g. in the case of P3HT with F_4TCNQ and F_6TCNNQ.[35] As a side remark, alignment by high temperature rubbing is an effective method to improve TE properties by increasing the both electrical conductivity and Seebeck coefficient in oriented polymer semiconductors.[8,10,35]

In this work, both D-A polymers **PAQM2T-TVT** and **PDPP2T-TVT** were aligned by high temperature rubbing and sequential doping was used to improve the TE properties of oriented films. The doping process was followed by polarized UV-vis-NIR spectroscopy and TEM. The anisotropic thermoelectric properties were measured as a function of doping level and for dopants with different locations in the semi-crystalline matrix of the two PSCs.

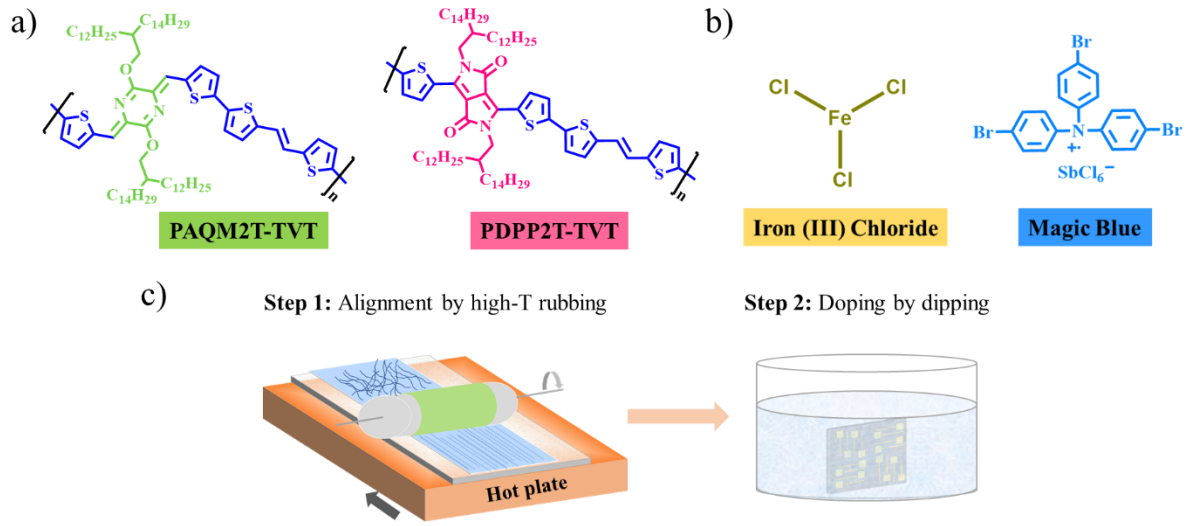

Figure 1. Chemical structures of a) the two donor-acceptor polymers **PAQM2T-TVT** and **PDPP2T-TVT** used in this study, b) dopants, c) Alignment of PAQM2T-TVT and PDPP2T-

TVT polymers by high-temperature rubbing and sequential doping in a solution of $FeCl_3$/nitromethane or MB/acetonitrile.

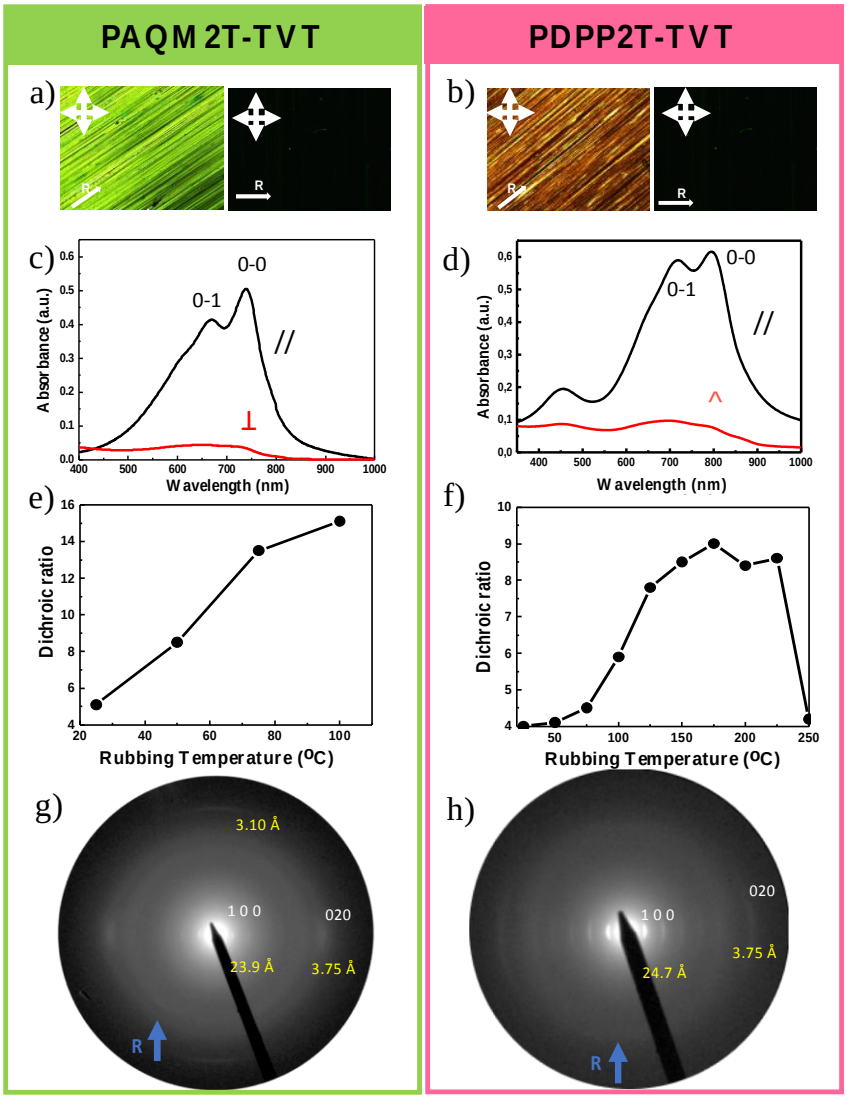

Figure 2. a) and b) Polarized optical microscopy images under crossed polarizers of the oriented thin films at 45° and 0° with respect to the rubbing direction (R) of **PAQM2T-TVT** and **PDPP2T-TVT**, respectively. The PAQM2T-TVT film obtained by rubbing at T = 100 °C and PDPP2T-TVT film obtained by rubbing at T = 175 °C. The rubbing direction R is indicated by a white arrow. c) and d) UV-vis spectra of the oriented thin films of **PAQM2T-TVT** and **PDPP2T-TVT** for light polarization parallel (//) and perpendicular (⊥) to the rubbing direction. e) and f) Evolution of the dichroic ratio *versus* T_R for **PAQM2T-TVT** and

PDPP2T-TVT, respectively. g) and h) ED pattern of pristine oriented **PAQM2T-TVT** and **PDPP2T-TVT** films, respectively.

2. Results and Discussion

2.1. Alignment of PAQM2T-TVT and PDPP2T-TVT

As reported in various studies, alignment of doped PSCs is beneficial for improving their thermoelectric properties[8,35] High temperature rubbing (HTR) is particularly effective to orient PSCs. In particular, the temperature at which the film is rubbed determines its ability to be aligned by rubbing. Therefore, we started to identify the best temperature for rubbing T_R for both polymers **PAQM2T-TVT** and **PDPP2T-TVT**. To this aim, we measured the dichroic ratio of the UV-vis-NIR absorption as a function of T_R. As illustrated in Figure 2, both polymers can be very well aligned with the highest dichroic ratio reaching 15 and 9 for **PAQM2T-TVT** and **PDPP2T-TVT**, respectively. There is a major difference between the two polymers concerning their thermomechanical properties: **PDPP2T-TVT** can be rubbed up to 240 °C contrary to **PAQM2T-TVT** for which mechanical degradation of the films is observed at temperatures beyond 100 °C that causes film delamination. Accordingly, the values of T_R leading to the best alignment for **PAQM2T-TVT** and **PDPP2T-TVT** are 100 °C and 175 °C, respectively. In order to overcome the limited range of rubbing temperatures for **PAQM2T-TVT**, we combined the rubbing step at 100 °C with a thermal annealing at 250 °C i.e. below the melting to achieve better structural order. Annealing for 1 min at 250 °C was found to be a good condition to observe high alignment and order in the **PDPP2T-TVT** films (see TEM electron diffraction in Figure 2).

Not only is the alignment modified by increasing T_R but also the structure of the films. This is manifested by the changes in the vibronic structure of the UV-vis-NIR spectra with T_R (see Figure S4). For both polymers, the absorbance of the *0-0* contribution in the vibronic structure increases substantially with T_R (especially for **PAQM2T-TVT**) suggesting

preferential J-type aggregates.[36,37] TEM investigations of similar D-A copolymers further showed that such aggregates involve segregated stacking of D and A units.[38]

The rubbed films of both polymers showed characteristic patterns of highly aligned films with coexistence of face-on and edge-on crystals with a common in-plane orientation of the chain direction imposed by rubbing. As noted in our previous study for PDPP-5T, limited structural order in the domains of **PDPP2T-TVT** is manifested by a very limited number of reflections in the ED patterns and in particular the absence of meridional 0 0 l reflections. In strong contrast, when the **PAQM2T-TVT** films are rubbed at 100 °C and annealed at 275 °C, they show a rather strong meridional reflection at 3.10 Å (indexed as 0 0 7). The π-stacking periodicities observed for both polymers are almost identical at 3.75 Å whereas the lamellar periodicities are 23.9 Å and 24.7 Å for **PAQM2T-TVT** and **PDPP2T-TVT**, respectively. To conclude, the growth conditions were identified to prepare highly oriented and ordered **PAQM2T-TVT** and **PDPP2T-TVT** films that are suitable to doping studies with $FeCl_3$ and MB in order to investigate the impact of doping amorphous/crystalline zones with these two dopants on the polarity switching mechanism.

2.2. Impact of doping concentration of $FeCl_3$ and MB on polaronic signatures in oriented thin films.

From the identified best conditions to achieve high orientation and ordering of the two polymers, we investigated their doping with the two dopants, $FeCl_3$ and MB by using polarized UV-vis-NIR spectroscopy (Table S1 in the SI collects the thickness and dichroic ratio of the films used hereafter). The incremental concentration doping (ICD) method was used to dope the oriented polymer films using solutions of the dopants of increasing concentration until a saturation of doping was manifested by a plateauing of the polaronic band intensities. Preliminary studies on the influence of doping time on the UV-vis-NIR

spectra of the films showed that doping times of 40s -1 min are sufficient to reach an equilibrium level of doping of the films for a given dopant concentration in solution.[8,35] As noted in the introduction, by changing the light polarization from parallel to perpendicular with respect to the rubbing direction, it is possible to probe preferentially doping in the ordered *versus* disordered polymer domains.

Firstly, focussing on spectroscopic signatures of doping for POL//R, the evolution of the UV–vis–NIR spectra of the $FeCl_3$ doped **PAQM2T-TVT** polymer is shown in figure 3a. For [$FeCl_3$]=0.1 mM, the neutral absorption of polymer was slightly decreased and no polaronic species were observed. Polaronic bands (P2 and P1 bands following the notations of Murrey et al.) appear for [$FeCl_3$] $\geq$ 0.5 mM and both bands increase in intensity with increasing doping level whereas bleaching of the neutral absorption of the polymer occurs.[39] Importantly, the P1 and P2 bands do not increase in absorbance at the same rate when the doping concentration increases. In Figure S5 we have plotted the ratio Abs(P2)/Abs(P1) of the absorbances of P2 and P1 bands *versus* doping concentration for $FeCl_3$ and MB (absorbance of P2 is measured at its maximum observed at low dopant concentration whereas for P1 it is measured at 2500nm). Clearly, there is a progressive decrease of the ratio with increasing [$FeCl_3$]. Following the work of Cavassin et al. and Enengl et al. on the doping of P3HT, a similar decrease in Abs(P2)/Abs(P1) was attributed to the formation of bipolarons in the disordered domains of the polymer at higher doping level[40,41,34] The situation for $FeCl_3$-doped **PDPP2T-TVT** is slightly different (figure 3e). The absorption of the neutral polymer is almost unchanged for [$FeCl_3$] = 0.6 mM. For [$FeCl_3$] = 3.0 mM, it starts bleaching and the polaronic bands P1 and P2 are formed (the P2 band is split for this polymer). A similar P2 band splitting was observed in DPP-based polymers doped with F_6TCNNQ and was assigned to a charge transfer complex (CTC) band.[26,42] However, $FeCl_3$ cannot form a CTC following the mechanism proposed by Mendez et al.[43] As a matter of facts, the P2 band component at

1380 nm tends to disappear with increasing [$FeCl_3$] suggesting that it is related to an oxidized species only present at low dopant concentration that transforms to a different species when the doping level increases. In contrast to **PAQM2T-TVT,** the neutral absorption of **PDPP2T-TVT** is not fully bleached at high [$FeCl_3$]. Moreover, the P2 band does not tend to disappear when increasing [$FeCl_3$] (see Figure S5) suggesting that less bipolarons are formed in **PDPP2T-TVT** than **PAQM2T-TVT** for the same range of investigated dopant concentrations. As a general observation, both polymers tend to lose their vibronic structure of the neutral absorption spectra upon doping. Recent work by Moulé and coworkers demonstrated that the formation of polarons on the polymer chains of D-A copolymers can disrupt the intra and/or inter-chain coupling that determines the intensities of the vibronic components of the exciton absorption of the neutral polymer.[44] A similar mechanism possibly accounts for the loss of vibronic structure in the absorption of the two investigated D-A polymers upon increasing doping concentration.

Considering the spectroscopic signatures of $FeCl_3$-doping for POL⊥R (Figure 3c and 3g), both polymers show a comparable bleaching of the neutral absorption band of amorphous domains upon doping with $FeCl_3$. However, the polaronic bands P1 and P2 are of weak absorbance contrary to what is seen for POL//R (especially for **PAQM2T-TVT**). Rather than well-defined bands, the spectra show a steady increase of a NIR absorbance up to 0.05-0.07 in the 1000-2500nm range. This observation suggests that $FeCl_3$ is doping the disordered domains of both **PDPP2T-TVT** and **PAQM2T-TVT**, similarly to the amorphous phases of P3HT and PBTTT.[10]

Finally, considering the doping of the two polymer films with magic blue, the UV-vis-NIR spectra of **PAQM2T-TVT** polymer are shown in figure 3b. Interestingly, a very low concentration of MB (0.06 mM) is sufficient to induce a full bleaching of the polymer absorption, concomitantly with the appearance of the polaronic bands P1 and P2. Eventually,

at very high [MB], the P2 band is almost fully removed. Upon increasing [MB], the P2 band intensity decreases at the expense of P1 more strongly than for $FeCl_3$ doping (see Figure S5.a) for equivalent dopant concentration in solution. The ratio Abs(P2)/Abs(P1) is seen to decrease very rapidly with MB concentration whereas for $FeCl_3$ it is more progressive. To reach similar low values of the ratio it is necessary to use very high $FeCl_3$ concentrations beyond 10 mM. Since the prevalence of the P1 band over P2 was considered as a fingerprint for bipolaron formation in disordered domains of P3HT, a similar conclusion is possible for MB-doped films of **PAQM2T-TVT**. Such a conclusion would further be consistent with the difference in the polarity switching between $FeCl_3$- and MB-doped polymer films.

The UV-vis-NIR spectra of MB doped **PDPP2T-TVT** (figure 3f) follows the same trend *versus* [MB] as **PAQM2T-TVT**. As expected, the neutral absorption of **PDPP2T-TVT** is bleached at ~90% for [MB] = 0.12 mM and polaronic bands are formed. By further increasing [MB], the neutral absorption of **PDPP2T-TVT** is almost fully bleached. The P1 band intensity was increasing with increasing the dopant concentration but a substantial intensity of the P2 band is retained at high [MB] similarly to the case observed when the films are doped with $FeCl_3$. Similarly to **PAQM2T-TVT**, doping **PAQM2T-TVT** with MB causes a rapid decrease of the ratio Abs(P2)/Abs(P1) (see Figure S5.b) suggesting preferential formation of bipolarons in disordered domains of the polymer. TEM analysis using electron diffraction will confirm that the preferential formation of bipolarons is consistent with MB not being located inside ordered domains but mainly in disordered zones of the polymer.

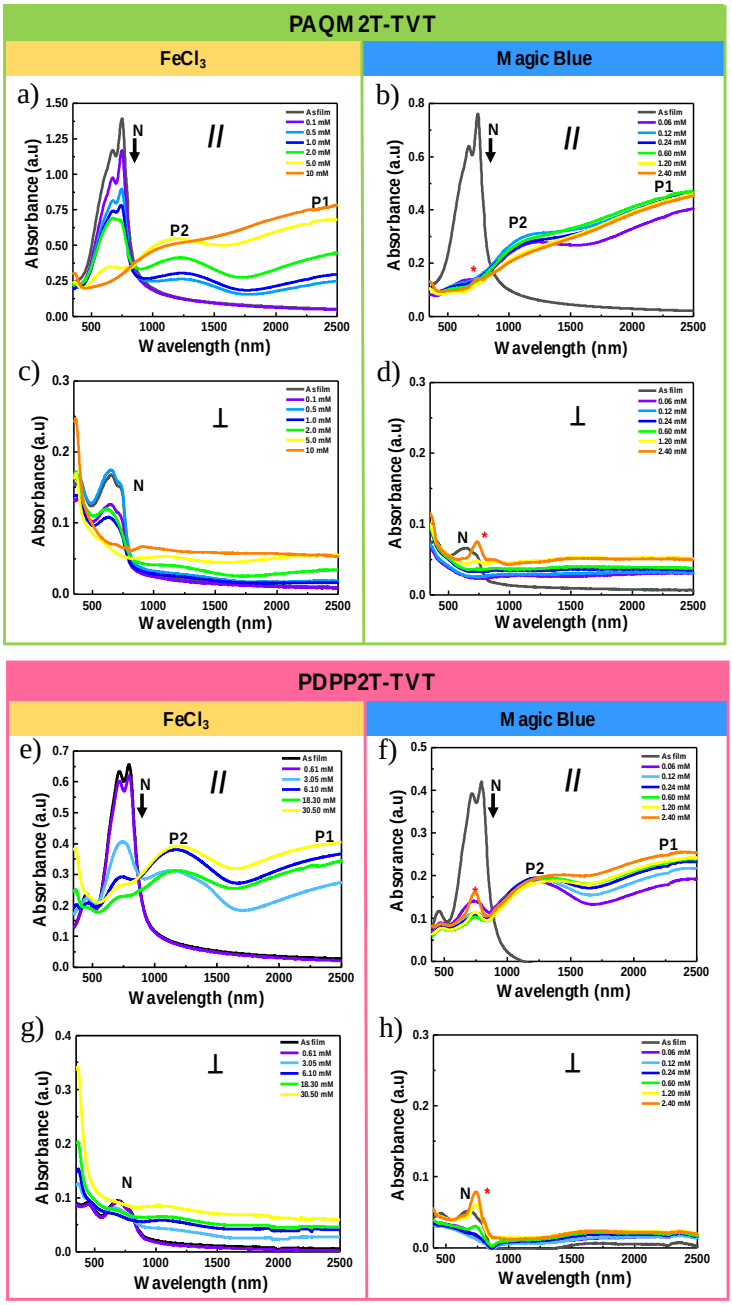

Figure 3. Evolution of the polarized UV–vis–NIR spectrum in oriented **PAQM2T-TVT** and **PDPP2T-TVT** thin films prepared by high-temperature rubbing and subsequently doped in solution of $FeCl_3$/nitromethane (a, c, e, g) and MB/acetonitrile (b, d, f, h). The light polarization is parallel (//) (a, b and e, f) and perpendicular (⊥) (c, d and g, h) to the rubbing direction. The red asterisk points at the 750nm band indicative of an excess of MB present on the film surface.

The situation for POL⊥R (Figure 3d and 3h) is instructive and quite similar to that seen for $FeCl_3$ doping. The absorption of **PAQM2T-TVT** and **PDPP2T-TVT** is fully bleached at a low concentration of MB, namely [MB] = 0.06 mM. However, the polaronic bands P1 and P2 are again difficult to see and replaced by a quasi-continuum of absorbance in the 1000-2500nm range. The latter may reflect the fact that chain conformations of the two polymers are strongly disordered in the amorphous phase, giving rise to a large distribution of HOMO and LUMO levels, thus a large energetic distribution of polaronic states with a correspondingly broad absorption spectrum.

2.3. Impact of Doping on the Structure of Oriented D-Q/A Polymers Probed by Electron Diffraction

To better understand the difference in the TE properties observed in MB- and $FeCl_3$-doped oriented films of **PAQM2T-TVT** and **PDPP2T-TVT**, we performed electron diffraction on aligned films doped at different concentrations. First, the optimal rubbing temperature was identified and second the films were subjected to incremental concentration doping (ICD). Figure S6 show the characteristic ED patterns of as-oriented and doped films of **PAQM2T-TVT** and **PDPP2T-TVT**. Figure 4 collects the cell parameters d_{100} and d_{020} (π-stacking periodicity) as a function of the MB and $FeCl_3$ concentrations.

First, the oriented films **PDPP2T-TVT** show a typical pattern of in-plane oriented films with a set of equatorial h 0 0 reflections coexisting with the 0 2 0 reflection and no clear reflection seen along the meridian. The films are thus made of a mixture of edge-on and face-on **PDPP2T-TVT** crystals with the chain direction parallel to the rubbing R. The absence of 0 0 l reflection is indicative of structural disorder in the chain direction within individual π-stacks of **PDPP2T-TVT**. Upon doping with $FeCl_3$, the unit cell shows a very strong lattice expansion in the chain direction with d_{010} increasing from ca. 25 Å in as-oriented films to almost 30 Å for doped films with 6.1 mM. The π-stacking periodicity is observed to increase

slightly between 3.7 Å and 4.1 Å for 6.1 mM. In the case of MB-doping, the situation is very different. First, the lattice is not showing any expansion in the side chain direction, but rather a slight contraction with d_{100} decreasing from 25 Å down to 23 Å. Second, the π-stacking is showing a contraction from 3.7 Å down to 3.3 Å. Accordingly, the crystal lattice of **PDPP2T-TVT** behaves very differently when doped with MB or with $FeCl_3$. In the case of MB-doping, the crystal lattice of **PDPP2T-TVT** seems to contract whereas in the case of $FeCl_3$ a strong expansion of the lattice is observed.

Let us observe the structural modification in the case of **PAQM2T-TVT**. In the case of $FeCl_3$-doping, **PAQM2T-TVT** behaves similarly to P3HT or PBTTT with a strong expansion of the lattice along the side chains (d_{100} from 23.9 Å in as-rubbed films to 27.4 Å at 2 mM $FeCl_3$) and a slight contraction of the π-stacking (from 3.65 Å to 3.47 Å). These observations suggest that $FeCl_3$ molecules are able to be intercalated inside the crystals of **PAQM2T-TVT**, as observed previously for other polythiophenes (P3HT and PBTTT).[10] The situation for MB-doping is again very different. Regardless of the MB concentration, d_{100} is almost unchanged. The π-stacking periodicity d_{020} shows a slight increase at low concentration and levels at a value identical to undoped films for [MB]=6 mM. Accordingly, the lattice of **PAQM2T-TVT** is almost unaffected by the doping with MB. This situation is fully consistent with the recent report on the structural changes evidenced for aligned P3HT doped with MB i.e. the absence of lattice modification upon doping.[34] In the case of P3HT doped with MB, TEM and polarized UV-vis-NIR spectroscopy showed that the MB dopants are preferentially located in the amorphous phase of P3HT and the crystals of P3HT are doped via their interface with the amorphous surrounding zones. A similar situation seems thus present in the case of **PAQM2T-TVT** when doped with MB. The situation evidenced for **PDPP2T-TVT** is slightly different from that of **PAQM2T-TVT** but there is a similarity for $FeCl_3$-doping, namely a strong lattice expansion in the side chain direction whereas no

such situation occurs for MB. Again, the overall results indicate that $FeCl_3$ dopants enter the crystals of **PDPP2T-TVT** whereas the contraction of the lattice when MB is used as a dopant suggests that MB molecules are not entering the crystals of **PDPP2T-TVT** and are thus preferentially located inside the amorphous phase of this polymer.

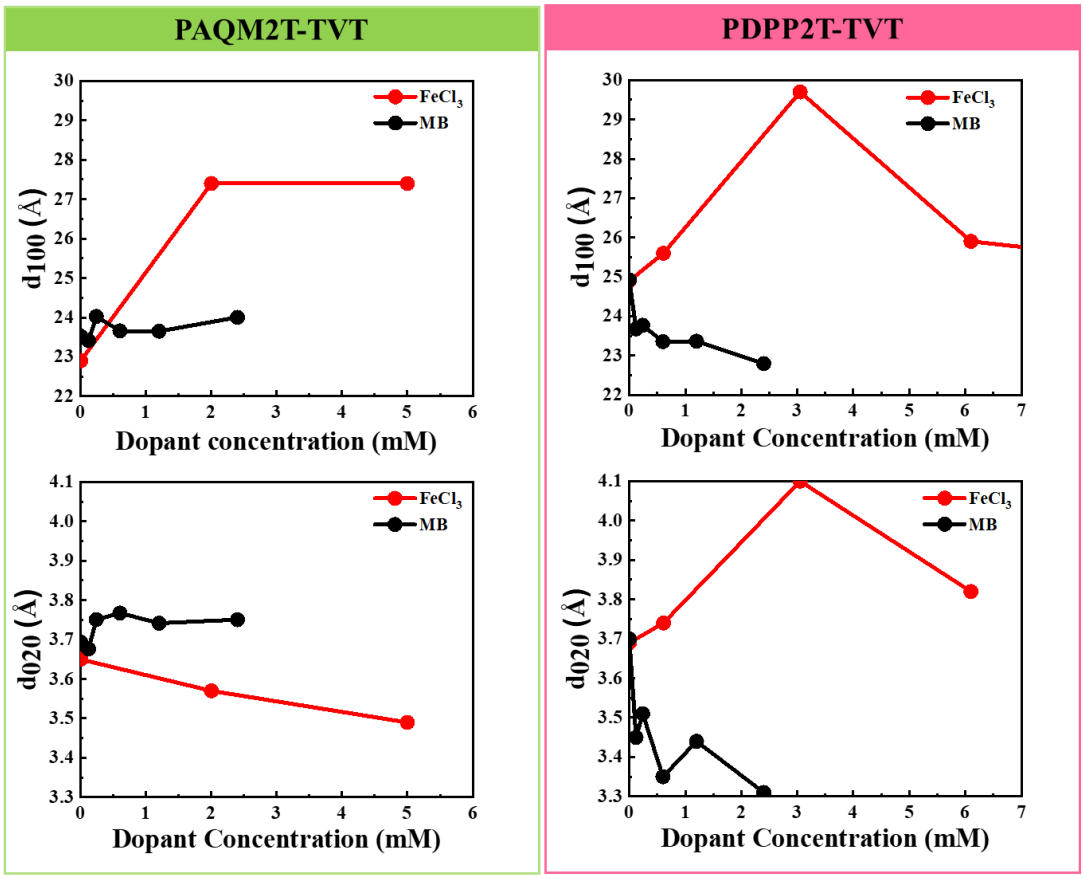

Figure 4. Variation of the lamellar periodicity d_{100} (along alkyl side chains) and the π-stacking periodicity d_{020} as a function of the dopant concentration of MB and $FeCl_3$ as observed in oriented films of **PAQM2T-TVT** and **PDPP2T-TVT**.

To conclude, TEM provides clear evidence that FeCl3 is intercalated inside the side chain layers of the two polymers. In strong contrast, when doped with MB, the crystal lattice of the two polymers is little changed, suggesting that MB molecules do not intercalate inside the crystals but are preferentially rejected to the amorphous zones. Doping of the polymer crystals must therefore occur through the interface with the disordered domains where the

MB dopant are preferentially located. This situation is again very similar to that observed for P3HT doped with MB.[34]

2.4. Anisotropic Thermoelectric Properties and polarity switching

Having evidenced differences in the dopant location of $FeCl_3$ and MB in the two polymers, let us see how it affects the thermoelectric properties (charge conductivity and Seebeck coefficient) of the oriented films and especially the mechanism of polarity switching.

The charge conductivity (σ) of oriented **PAQM2T-TVT** and **PDPP2T-TVT** polymer films *versus* $FeCl_3$ and MB are shown in figure 5. Let us first focus on the impact of $FeCl_3$ doping on charge conductivity in oriented **PAQM2T-TVT** and **PDPP2T-TVT**. In both polymers σ reaches a maximum value at intermediate doping levels and after that it decreased quite abruptly for high [$FeCl_3$], similarly to what has been observed previously for PDPP5T doped with $FeCl_3$.[17] A maximum conductivity of 88 S/cm is achieved in the chain direction for **PAQM2T-TVT** doped polymer at a dopant concentration of around 2 mM. In the case of **PDPP2T-TVT** the maximum σ was 113 S/cm in the chain direction at a dopant concentration of 6.1 mM.

Doping the two polymers with MB reveals important differences. First, it is observed that the maximum of charge conductivity is reached at a much lower concentration for MB than for $FeCl_3$. As an example, in oriented **PAQM2T-TVT** polymer films, σ reached a maximum value (782 S/cm) for [MB] = 0.12 mM. This is fully consistent with the UV-vis-NIR results indicating that bleaching of the neutral polymer peak occurs at much lower [MB] as compared to $FeCl_3$. Increasing [MB] to 0.24 mM leads to a reduction of the charge conductivity to 154 S/cm. Similarly, to **PAQM2T-TVT**, MB-doping of oriented **PDPP2T-TVT** occurs at very low concentration of 0.06 mM and results in a step increase of

conductivity up to 119 S/cm. Doping further increases σ to 443 S/cm at 0.6 mM. As for the other polymer, the conductivity finally decreases at larger [MB]. Accordingly, MB-doping of both polymers is clearly different from $FeCl_3$-doping in the sense that: i) very low concentrations of MB are sufficient to dope substantially the two polymers and ii) conductivities in MB-doped films are larger than for $FeCl_3$-doped films. The same behaviour was observed in the case of P3HT and was attributed to the preferential location of dopants in the amorphous P3HT domains that preserves thus the perfection of P3HT crystals. This is consistent with the present TEM findings for the two polymers **PAQM2T-TVT** and **PDPP2T-TVT** showing no clear sign of dopant intercalation into crystalline domains. Hence, as for P3HT, one may consider that, for similar oxidation levels, the larger conductivities found for MB-doped systems relate to the better preservation of order within crystalline domains, hence larger charge mobilities. In addition, Coulomb trapping of carriers within ordered domains is possibly reduced since the $SbCl_6^-$ counterions locate preferentially into amorphous domains, increasing thus the average distance between dopant counterion ($SbCl_6^-$) and the polaronic charges in the ordered domains.

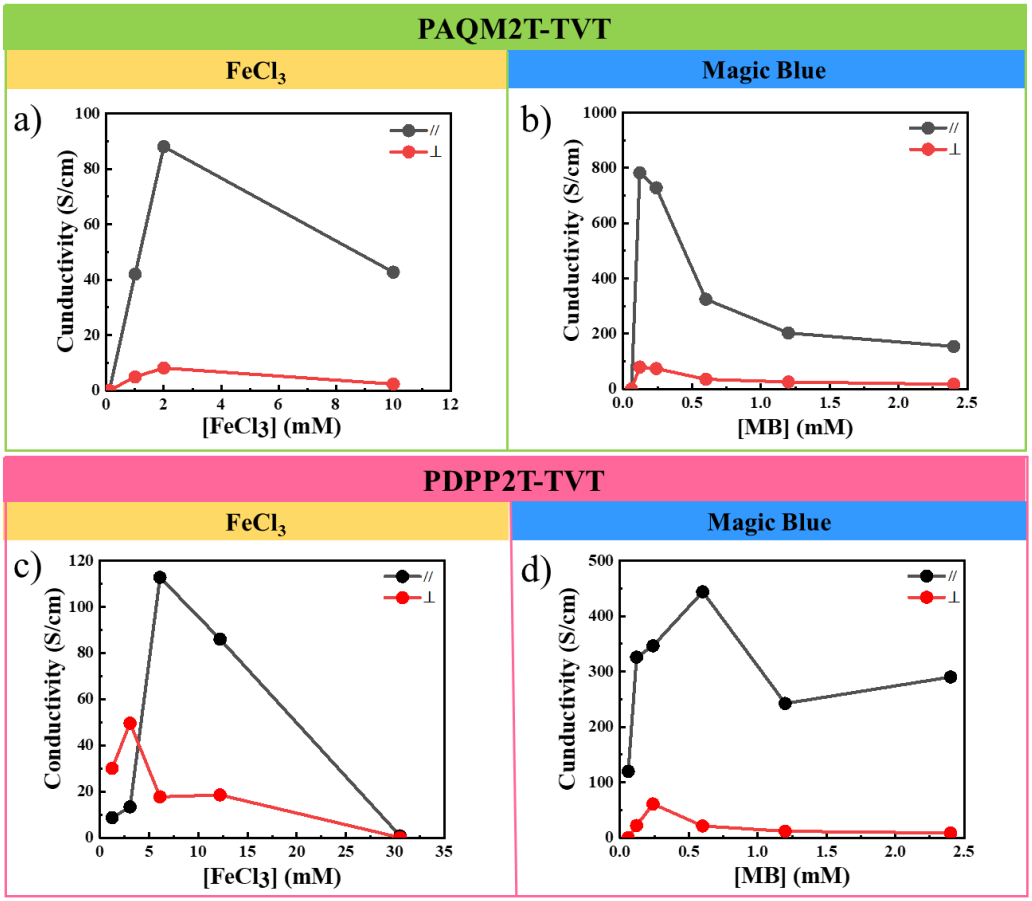

Figure 5. Evolution of the anisotropic charge conductivity in oriented **PAQM2T-TVT** and **PDPP2T-TVT** thin films aligned by high temperature rubbing as a function of the dopant concentration for $FeCl_3$ (a and c) and MB (b and d). The lines are just guide for the eyes.

Let us observe how the doping with $FeCl_3$ and MB affects the Seebeck coefficient of the oriented films of **PAQM2T-TVT** and **PDPP2T-TVT**. The evolution of the Seebeck coefficient (*S*) of oriented **PAQM2T-TVT** and **PDPP2T-TVT** films *versus* $FeCl_3$ and MB concentration is shown in Figure 6. In the case of $FeCl_3$ doping, there is a very clear polarity switching of the Seebeck coefficient for the two polymers. Moreover, as shown in our previous work, the polarity switching occurs at a $FeCl_3$ concentration corresponding to the maximum of charge conductivity: The polarity switching is observed for both directions parallel and perpendicular to the chains. The Seebeck coefficient (*S*) decreases with increasing dopant concentration ($FeCl_3$ and MB). In strong contrast, no polarity switch occurs

in oriented **PAQM2T-TVT** when doped with MB. The Seebeck coefficient decreases from 147 μV K^{-1} at [MB] = 0.06 mM i.e. at the maximum of conductivity (see Figure S7). Upon further doping, the Seebeck coefficient levels to a value close to 0 (0.24 μV K^{-1} for [MB] = 2.4 mM) without change of polarity. The same trend was observed for oriented films of **PDPP2T-TVT** although for [MB]=1.25 mM the Seebeck coefficient became slightly negative but close to 0 within error margins. Accordingly, for both polymers, at high [MB], the Seebeck coefficient reaches a plateau close to 0. In no case can we observe negative Seebeck coefficients of several tens of μV/K as for the $FeCl_3$-doped films.

Our experiments demonstrate that the Seebeck coefficient of MB-doped polymers is not switching polarity although similar oxidation levels are reached as for $FeCl_3$-doped films. As in the case of MB-doped P3HT, TEM provides evidence that the MB dopant do not induce a substantial lattice expansion that is the fingerprint of dopant intercalation in the crystals of the polymer.[34] The absence of lattice expansion indicates that MB is not entering the ordered domains of **PAQM2T-TVT** and **PDPP2T-TVT**. Contrary to MB, other dopants such as $NoBF_4$ or $FeCl_3$ do enter the lattice of low bandgap polymers (see schematic illustration in figure 7).[25,26] Accordingly, the present study identifies the dopant intercalation into crystalline domains of the polymers as a necessary condition to observed the switching of the Seebeck's sign upon doping. As noted in our previous contribution, the ambipolar character of DPP-based alternated copolymers is not a sufficient condition to observe switching of the Seebeck sign from p to n upon strong p-type doping.[26] When the dopant locates essentially in the disordered or amorphous phase of the polymer, for dopants such as MB, no polarity switching is observed. This result suggests that the negative sign of the Seebeck is associated with the band filling mechanism in the more ordered phase rather than to a difference in the transport between crystalline and amorphous phases that changes with doping level.

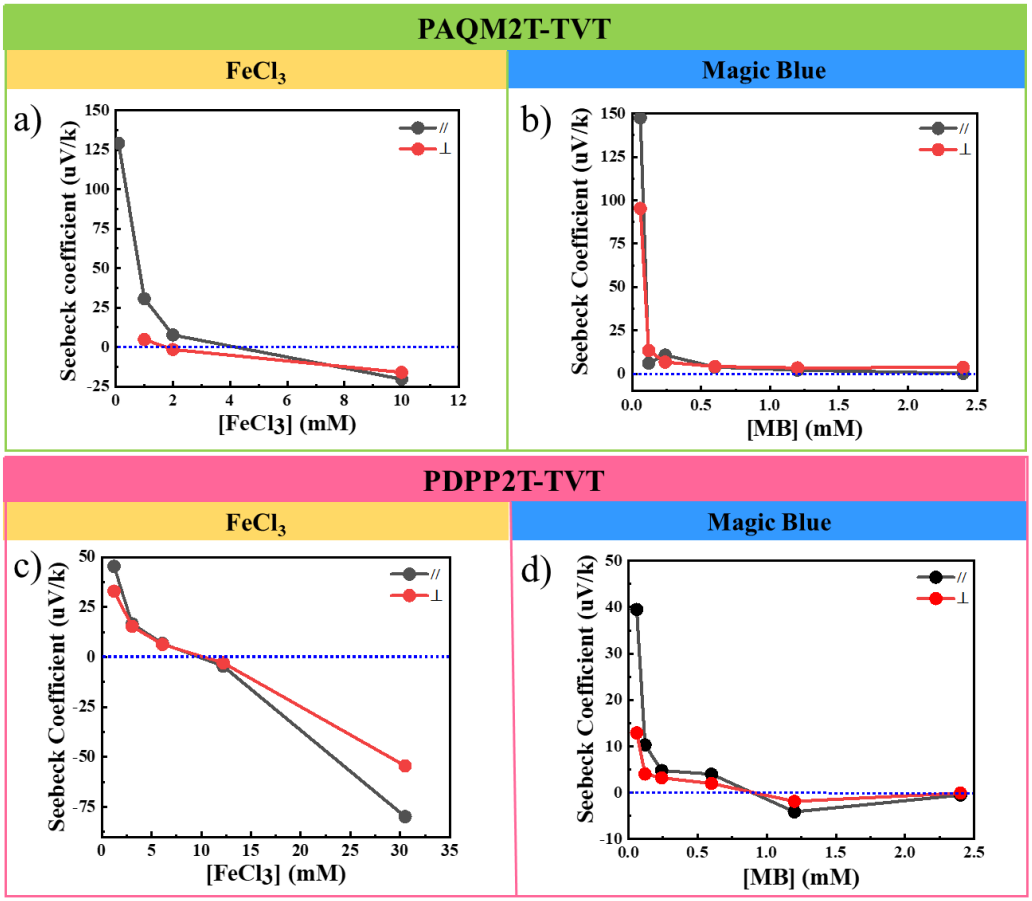

Figure 6. Evolution of the anisotropic Seebeck coefficient (*S*) of oriented **PAQM2T-TVT** and **PDPP2T-TVT** thin films aligned by high temperature rubbing after sequential doping in solution of increasing concentration $FeCl_3$ (a, c) and MB (b, d).

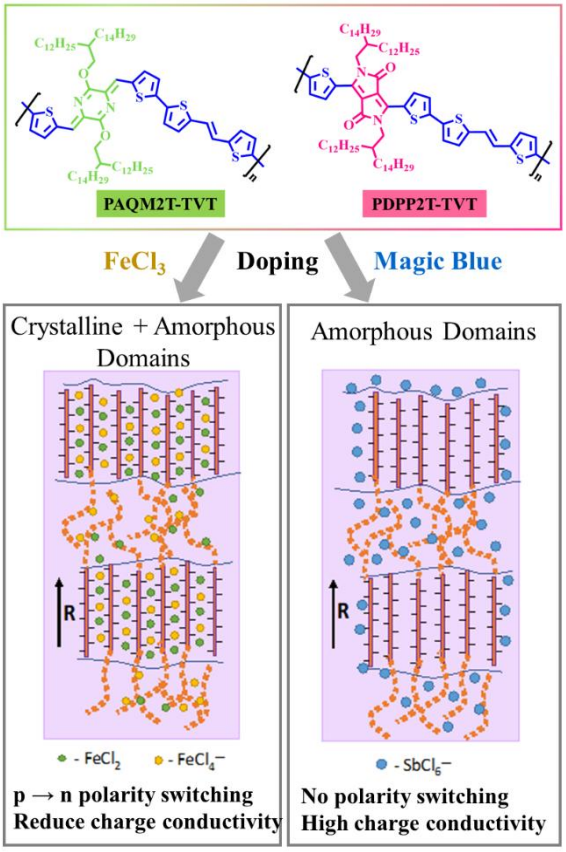

Figure 7. Schematic illustration of the impact of dopant location on the thermoelectric properties of two low bandgap polymers (**PAQM2T-TVT** and **PDPP2T-TVT**) and in particular on the occurrence of the polarity switching mechanism of the Seebeck coefficient. This switching phenomenon is only observed for polymers for which dopants are located inside the ordered domains of the polymer ($FeCl_3$ or $NOBF_4$). In strong contrast, a dopant such as Magic blue is unable to induce polarity switching upon doping.

3. Conclusion.

Several groups observed that p-type doping of low bandgap polymers can induce a switching of the sign of the Seebeck coefficient. It was previously proposed that the switching could be

the result of a differential doping of the amorphous *versus* crystalline phases of the polymer.[25] In this work, we demonstrate that the absence of dopants inside the polymer crystals of **PAQM2T-TVT** and **PDPP2T-TVT** impedes the p $\rightarrow$ n polarity switching mechanism. This is observed when two low bandgap polymers are doped with magic blue, whereas dopants such as $FeCl_3$ or $NOBF_4$ can enter polymer crystals and induce polarity switching. Accordingly, the oxidation level of the PSC that determines band filling is not the only parameter that controls polarity switching in low bandgap polymers. This result is very important as it demonstrates that the chemical nature of the dopant and its ability to be present/absent in crystalline and/or amorphous phases of a PSC has major impacts on the physics of charge transport and thermoelectric properties. The objective to identify specific dopants that can dope preferentially and exclusively the amorphous or the crystalline domains of a PSC could thus be an interesting strategy to tune thermoelectric properties in thin films of doped PSCs.

Acknowledgments.

We thank the TEM platform (M. Schmutz) from ICS for technical support. Support from ANR through grant THERMOPOLYS (MB and BS) and Région Centre-Val-De-Loire through grant ETHERMO (BS) is acknowledged. Catherine Saettel is acknowledged for performing the DSC measurements. Christophe Contal is acknowledged for performing the AFM measurements. We want also to thank Bernard Lotz and Olivier Bardagot for a critical reading of the manuscript.

Conflict of interest

The authors declare no conflict of interest

Author contributions

B. Dyaga, B. Schmaltz and M. Brinkmann led the project, designed the experiments, and wrote the manuscript. B. Dyaga carried out the synthesis of the monomers and polymers as well as the characterizations. A. Lemaire carried out the alignment of the polymers by rubbing, the doping process and TE measurements. S. Guchait performed the optical spectroscopy and assisted with the TE measurements. H. Zeng assisted with the doping process and the optical spectroscopy. B. Schmaltz designed the polymers. M. Brinkmann performed the electron diffraction analysis. All the authors have given approval to the final version of the manuscript.

References

1. R. Kroon, D. A. Mengistie, D. Kiefer, J. Hynynen, J. D. Ryan, L. Yu, and C. Müller, *Chem. Soc. Rev.*, 2016, **45,** 6147.
2. O. Bubnova, and X. Crispin, *Energy Environ. Sci.*, 2012, **5,** 9345.
3. T. Degousée, V. Untilova, V. Vijayakumar, X. Xu, Y. Sun, M. Palma, M. Brinkmann, L. Biniek and O. Fenwick, *J. Mater. Chem. A*, 2021, **9**, 16065–16075.
4. G. Zuo, H. Abdalla, and M. Kemerink, *Adv. Electron. Mater.*, 2019, **5,** 1800821.
5. R. Kroon, D. Kiefer, D. Stegerer, L. Yu, M. Sommer, and C. Müller, *Adv. Mater.*, 2017, **29,** 1700930.
6. J. Hynynen, D. Kiefer, L. Yu, R. Kroon, R. Munir, A. Amassian, M. Kemerink, and C. Müller, *Macromolecules*, 2017, **50,** 8140.
7. A. M. Glaudell, J. E. Cochran, S. N. Patel, and M. L. Chabinyc, *Adv. Energy Mater.*, 2015, **5,** 1401072.
8. A. Hamidi-Sakr, L. Biniek, J.-L. Bantignies, D. Maurin, L. Herrmann, N. Leclerc, P. Leveque, V. Vijayakumar, N. Zimmermann, and M. Brinkmann, *Adv. Funct. Mater.*, 2017, **27,** 1700173.

9. Z. Liang, Y. Zhang, M. Souri, X. Luo, A. M. Boehm, R. Li, Y. Zhang, T. Wang, D.-Y. Kim, J. Mei, S. R. Marder and K. R. Graham, *J. Mater. Chem. A*, 2018, **6**, 16495–16505.

10. V. Vijayakumar, Y. Zhong, V. Untilova, M. Bahri, L. Herrmann, L. Biniek, N. Leclerc, and M. Brinkmann, *Adv. Energy Mater.*, 2019, **9,** 1900266

11. I. E. Jacobs and A. J. Moulé, *Advanced Materials*, 2017, **29**, 1703063.

12. D. T. Scholes, P. Y. Yee, J. R. Lindemuth, H. Kang, J. Onorato, R. Ghosh, C. K. Luscombe, F. C. Spano, S. H. Tolbert and B. J. Schwartz, *Advanced Functional Materials*, 2017, **27**, 1702654.

13. W. Zhao, J. Ding, Y. Zou, C. Di and D. Zhu, *Chem. Soc. Rev.*, 2020, **49**, 7210–7228.

14. A. D. Scaccabarozzi, A. Basu, F. Aniés, J. Liu, O. Zapata-Arteaga, R. Warren, Y. Firdaus, M. I. Nugraha, Y. Lin, M. Campoy-Quiles, N. Koch, C. Müller, L. Tsetseris, M. Heeney and T. D. Anthopoulos, *Chem. Rev.*, 2022, **122**, 4420–4492.

15. A. Tripathi, Y. Lee, S. Lee and H. Y. Woo, *J. Mater. Chem. C*, 2022, **10**, 6114–6140.

16. Y. Sun, C. A. Di, W. Xu, and D. Zhu, *Adv. Electron. Mater.*, 2019, **5,** 1800825.

17. Y. Lu, J. Y. Wang, and J. Pei, *Chem. Mater.*, 2019, **31,** 6412-6423.

18. S. Griggs, A. Marks, H. Bristow and I. McCulloch, *J. Mater. Chem. C*, 2021, **9**, 8099–8128.

19. S. Deng, C. Dong, J. Liu, B. Meng, J. Hu, Y. Min, H. Tian, J. Liu and L. Wang, *Angewandte Chemie International Edition*, 2023, **62**, e202216049.

20. K. Feng, J. Wang, S. Y. Jeong, W. Yang, J. Li, H. Y. Woo and X. Guo, *Advanced Science*, 2023, **n/a**, 2302629.

21. R. A. Schlitz, F. G. Brunetti, A. M. Glaudell, P. L. Miller, M. A. Brady, C. J. Takacs, C. J. Hawker, and M. L. Chabinyc, *Adv. Mater.*, 2014, **26,** 2825-2830.

22. S. Wang, H. Sun, U. Ail, M. Vagin, P. O. Å. Persson, J. W. Andreasen, W. Thiel, M. Berggren, X. Crispin, D. Fazzi and S. Fabiano, *Adv. Mater.*, 2016, **28**, 10764–10771.

23. J. Liu, G. Ye, B. V. D. Zee, J. Dong, X. Qiu, Y. Liu, G. Portale, R. C. Chiechi, and L. J. A. Koster, *Adv. Mater.*, 2018, **30,** 1804290.

24. H. Guo, C.-Y. Yang, X. Zhang, A. Motta, K. Feng, Y. Xia, Y. Shi, Z. Wu, K. Yang, J. Chen, Q. Liao, Y. Tang, H. Sun, H. Y. Woo, S. Fabiano, A. Facchetti and X. Guo, *Nature*, 2021, **599**, 67–73.

25. Z. Liang, H. H. Choi, X. Luo, T. Liu, A. Abtahi, U. S. Ramasamy, J. A. Hitron, K. N. Baustert, J. L. Hempel, A. M. Boehm, A. Ansary, D. R. Strachan, J. Mei, C. Risko, V. Podzorov, and K. R. Graham *Nat. Mater.*, 2021, **20,** 518-524.

26. H. Zeng, M. Mohammed, V. Untilova, O. Boyron, N. Berton, P. Limelette, B. Schmaltz, and M. Brinkmann, *Adv. Electron. Mater.*, 2021, **7,** 2000880.

27. J. Wang, Y. Wang, Q. Li, Z. Li, K. Li, and H. Wang, *CCS Chemistry*, 2021, **3,** 2482-2493.

28. S. Hwang, W. J. Potscavage, Y. S. Yang, I. S. Park, T. Matsushima, and C. Adachi, *Phys. Chem. Chem. Phys.*, 2016, **18,** 29199-29207.

29. K. Xu, T. P. Ruoko, M. Shokrani, D. Scheunemann, H. Abdalla, H. Sun, C. Y. Yang, Y. Puttisong, N. B. Kolhe, J. S. M. Figueroa, and J. O. Pedersen, T. Ederth, W. M. Chen, M. Berggren, S. A. Jenekhe, D. Fazzi, M. Kemerink and S. Fabiano, *Adv. Funct. Mater.*, 2022, **32,** 2112276.

30. B. Dyaga, S. Mayarambakam, O. A. Ibraikulov, N. Zimmermann, S. Fall, O. Boyron, T. Heiser, N. Leclerc, N. Berton, and B. Schmaltz, *Mater. Adv.*, 2022, **3,** 6853-6861.

31. H. Chen, Y. Guo, G. Yu, Y. Zhao, J. Zhang, D. Gao, H. Liu, and Y. Liu, *Adv. Mater.*, 2012, **24,** 4618-4622.

32. A. I. Hofmann, R. Kroon, S. Zokaei, E. Järsvall, C. Malacrida, S. Ludwigs, T. Biskup and C. Müller, *Advanced Electronic Materials*, 2020, **6**, 2000249.

33. S. Zhang, H. M. Hill, K. Moudgil, C. A. Richter, A. R. Hight Walker, S. Barlow, S. R. Marder, C. A. Hacker and S. J. Pookpanratana, *Advanced Materials,* 2018, **30**, 1802991.

34. Y. Zhong, V. Untilova, D. Muller, S. Guchait, C. Kiefer, L. Herrmann, N. Zimmermann, M. Brosset, T. Heiser, and M. Brinkmann, *Adv. Funct. Mater.,* 2022, **32,** 2202075.

35. V. Untilova, H. Zeng, P. Durand, L. Herrmann, N. Leclerc and M. Brinkmann, *Macromolecules*, 2021, **54**, 6073–6084.

36. N. J. Hestand and F. C. Spano, *Chem. Rev.*, 2018, **118**, 7069–7163.

37. F. C. Spano and C. Silva, *Annu. Rev. Phys. Chem.*, 2014, **65**, 477–500.

38. Y. Zhong, L. Biniek, N. Leclerc, S. Ferry and M. Brinkmann, *Macromolecules,* 2018, **51**, 4238–4249.

39. T. L. Murrey, M. A. Riley, G. Gonel, D. D. Antonio, L. Filardi, N. Shevchenko, M. Mascal and A. J. Moulé, *J. Phys. Chem. Lett.*, 2021, **12**, 1284–1289.

40. P. Cavassin, I. Holzer, D. Tsokkou, O. Bardagot, J. Réhault and N. Banerji, *Advanced Materials*, 2023, **35**, 2300308.

41. C. Enengl, S. Enengl, S. Pluczyk, M. Havlicek, M. Lapkowski, H. Neugebauer and E. Ehrenfreund, *ChemPhysChem*, 2016, **17**, 3836–3844.

42. Y. Karpov, T. Erdmann, M. Stamm, U. Lappan, O. Guskova, M. Malanin, I. Raguzin, T. Beryozkina, V. Bakulev, F. Günther, and S. Gemming, *Macromolecules*, 2017, **50,** 914-926.

43. H. Méndez, G. Heimel, S. Winkler, J. Frisch, A. Opitz, K. Sauer, B. Wegner, M. Oehzelt, C. Röthel, S. Duhm, D. Többens, N. Koch and I. Salzmann, *Nature Communications*, 2015, **6**, 8560.
44. A. J. Moulé, G. Gonel, T. L. Murrey, R. Ghosh, J. Saska, N. E. Shevchenko, I. Denti, A. S. Fergerson, R. M. Talbot, N. L. Yacoub, M. Mascal, A. Salleo and F. C. Spano, *Advanced Electronic Materials*, 2022, **8**, 2100888.